RSC Advances

ROYAL SOCIETY OF CHEMISTRY

www.rsc.org/advances

RSC Advances

ARTICLE

Improvement of mechanical performance of solution styrene butadiene rubber by controlling the concentration and the size of in-situ derived sol-gel silica particles

Received 00th January 20xx,
Accepted 00th January 20xx

DOI: 10.1039/x0xx00000x

www.rsc.org/

V. Sankar Raman[a,b], A. Das[a,c], K. W. Stöckelhuber[a*], S. B. Eshwaran[a,b], J. Chanda[a,b], M. Malanin[a], U. Reuter[a], A. Leuteritz[a], R. Boldt[a], , S. Wießner[a,b], G. Heinrich [a,b]

Incorporation of precipitated silica rubber compound is now a standard technology in energy efficient green tire manufacturing process. In the present work silica nanoparticles were generated by in-situ sol-gel technique in solution styrene butadiene rubber (SSBR) using tetraethylorthosilicate (TEOS) as silica precursor. A full control over the amount of silica and size of the silica particles is realized while maintaining a good distribution and dispersion level of the nano-silica particles. In present case the amount of synthesized silica were varied from 10-50 phr (parts per hundred) and the particles size remains in the range of 200-300 nm. The in-situ silica based rubber composites offer better processing characteristics as compared with standard commercial precipitated silica at same loading level. The reinforcing character of in-situ silica was further enhanced by the use of a silane coupling agent, i.e. bis [3-(triethoxysilyl) propyl] tetrasulfide (TESPT). Various instrumental techniques, such as tensile test, dynamic mechanical analysis and strain sweep analysis, abrasion test, rebound test and Mooney viscometry reveal superior mechanical performance and good processability of the in-situ silica composites. Scanning and transmission electron microscopy studies indicate that the particle size distribution remains in the same range irrespective of the concentration of the silica particles.

Introduction

Reinforcement of rubbers by addition of fillers is a most common technique to exploit different soft polymeric materials in several technological applications starting from high performance vehicle tires to floor mats. Plenty of organic and inorganic materials can be utilized to improve the performance of rubbers. Carbon black is one of the major reinforcing materials holding its share since nineteenth century. Reinforcement by carbon black is mainly achieved through high surface area, smaller particle size and higher surface activity of carbon black particles that result in a strong rubber-filler interaction[1-4]. Especially in research for the past few decades, nanofillers from inorganic origin like precipitated or fumed silica, nanoclay[5, 6], layered double hydroxide[7] and halloysite nanotubes[8] have been used as reinforcing agents in rubber compounds. These inorganic nanofillers offer very good mechanical reinforcement even at low volume fractions. Amongst various inorganic fillers, precipitated silica is widely used and well accepted in the field of tire technology. The reinforcing capability of silica can only be experienced when a silane coupling agent is used in the rubber compounding process[9, 10]. Silica filled tires become more popular in terms of low rolling resistance, improved wet grip and skid resistance compared to conventional carbon black filled tires[11, 12]. Even though silica technology is successfully being practiced in industries, some issues are still encountered while using silica as fillers in rubbers. One of the major issues is poor nanoscale dispersion of the silica in highly filled rubber composites[13-16]. To address this problem the generation of silica particles by sol-gel method offers new possibilities to achieve reinforcing silica particles inside the rubber matrix by simple chemical reactions[17, 18]. The schematic of such a sol-gel reaction and silica particles formation is given in Scheme 1. Several techniques are developed to produce sol-gel silica particles inside the polymer which are mainly based on latex blending[19, 20], solution technique[21] and swelling of rubber matrix in silica precursors[17, 22]. Mostly in latex blending technique, the final composites show poor particle growth and mechanical properties. Swelling technique has been explored very rapidly in the last two decades because of its ease of processing, controlled particles growth and low agglomeration tendencies. Recently the in-situ silica nanoparticles are prepared by swelling of pre-molded un-vulcanized rubbers with particular dimension on TEOS and immersed spontaneously in a catalyst solution[23, 24]. In most of the literature sol-gel silica were synthesized by swelling vulcanized or unvulcanized rubber in tetraorthosilicate (TEOS) based precursor solution[17, 19, 22, 23, 25-27]. Generating silica particles in a vulcanized rubber material cannot be a good practice for industries as it deforms the shape of the final rubber product.

[a] Leibniz-Institut für Polymerforschung Dresden e. V., Hohe Strasse 6, 01069 Dresden, Germany.
[b] Technische Universität Dresden, Institut für Werkstoffwissenschaft, 01062 Dresden, Germany
[c] Technical University of Tampere, Korkeakoulunkatu 16, 33101 Tampere, Finland
* stoeckelhuber@ipfdd.de.

In the present study we have followed the sol-gel route to generate silica nanoparticles inside an uncrosslinked SSBR matrix to overcome the above-mentioned issues. In present case the amounts as well as the size of the silica particles are controlled by tuning of reaction conditions.

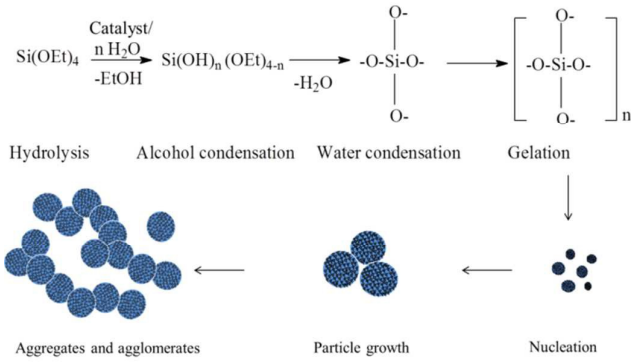

Scheme 1: Silica particle formation through sol-gel reaction

Experimental

Materials

Solution styrene butadiene rubber (SSBR) BUNA 2525-0 VSL HM containing 25 % vinyl content, 25% styrene content, N-cyclohexyl,2-benzothioazolesulfonamide (CBS) and diphenyl-guanidine (DPG) were kindly provided by Lanxess chemicals Ltd, Germany. Zinc oxide, stearic acid, sulfur, Tetrahydrofuran (THF) and N-butylamine were obtained from Acros Organics, Germany. The silica precursor tetraethoxyorthosilicate (TEOS) with a purity of 99 % was purchased from Sigma Aldrich. The silane coupling agent bis[3-(triethoxysilyl) propyl] tetrasulfide (TESPT) and precipitated silica (Ultrasil-VN3) were kindly supplied by Evonik Industries (Essen, Germany) having a purity of 99 %.

Preparation of silica-rubber composites

The preparation of SSBR-silica composites was carried out in two stages. In the first stage, silica-rubber masterbatches were prepared. To a rubber solution with 30 g of SSBR in 300 ml of THF, 0.1 mole of TEOS and 0.2 moles of water were added in a round bottom flask. Then 0.025 moles of n-butyl amine was added as a catalyst and the whole homogenous mixture was stirred and refluxed for 4 hours at 60 °C. The obtained white viscous solution mixture was ultrasonicated for 10 min to avoid the pre-agglomeration of silica particles. The sonicated solution was then slowly poured into 900 ml of ethanol to solidify and precipitate the silica-rubber phase immediately. The precipitated mass was collected by simple filtering process, washed with ethanol and dried for 48 hours at 30°C in hot air oven to evaporate the trace solvents. The dried mass contained only the SSBR matrix with sol-gel silica nanoparticles. By varying the quantity of TEOS and water (with the same mole ratio of 1:2) different volume fractions of silica in rubber were prepared and quantified by TGA.

In the second stage the rubber-silica masterbatches were compounded with other rubber chemicals. Two step mixing process was followed to incorporate the rubber chemicals. In the first step, along with the SSBR/in-situ-silica masterbatch, an appropriate amount of raw SSBR was added into a internal mixer to achieve the fill factor of mixing chamber (Haake Rheomix 600P, fill factor of 0.7 which corresponds to 56 cm^3 volume). After sufficient mixing, other ingredients were sequentially added: zinc oxide (2 phr), stearic acid (3 phr) and the required amount of TESPT coupling agent (1 phr of TESPT for every 10 phr of silica). The compounding was performed at 110 °C and 80 rpm for 6 min and dumped at an average temperature of ~140 °C. In a second step, the vulcanizing chemicals CBS (1.4 phr), DPG (1.7 phr) and sulfur (1.4 phr) were added at a two roll mill (Polymix-110L, Servitec Maschinen Service GmbH, Wustermark, Germany) at 50 °C with a constant friction ratio of 1:1.2. The samples were then allowed to mature for 24 hours at room temperature. The matured samples were subjected to rheometric study by a rubber process analyzer (Scarabaeus SIS-V50, Scarabaeus GmbH, Wetzlar, Germany) to find the optimum cure time. The compounds were vulcanized into sheets of 2 mm thickness at 160 ˚C by the use of a compression molding press.

In the sample abbreviations (e.g.: i10, i10s, i30, i30s etc.), 'i' represents in-situ silica compound, the number is the amount of silica in phr (parts per hundred of rubber) and the suffix 's' represent the compounds containing TESPT silane coupling agent.

Characterization of silica-SSBR nanocomposites

The amount of silica in the rubber compounds was investigated by thermogravimetry (TGA Q 5000 from TA instruments, New Castle, DE, USA) at a heating rate of 20 K/min under nitrogen atmosphere up to 600 °C and then under oxygen atmosphere from 600-800 °C. From the samples containing only silica and rubber, the quantitative content of silica and the conversion of silica from the precursor can be calculated by the following simple expressions:

$$\textbf{\textit{Silica content}}\ (\%) = \frac{\textbf{\textit{weight of residue}}}{\textbf{\textit{weight of composite}}} \times \mathbf{100} \qquad (1)$$

$$\textbf{\textit{Conversion}}\ (\%) = \frac{\textbf{\textit{experimental amount of }}\boldsymbol{SiO_2}}{\textbf{\textit{theoritical amount of }}\boldsymbol{SiO_2}} \times \mathbf{100} \qquad (2)$$

To study the silica formation in rubber, solution samples were taken at different periods of time and poured immediately into ethanol. The solidified mass was dried at 30˚C for 2 hours and used for further Fourier transform infrared (FTIR) analysis. To separate the *in-situ* prepared silica powder the final reaction mixture was poured into THF and washed by means of centrifugation process for 5 cycles. Attenuated total reflection (ATR) FTIR spectra were taken using a Vertex 80v spectrometer (Bruker) equipped with both

HgCdTe-detector and Golden Gate ATR-unit (Specac). The spectral region was 4000-600 cm^{-1} and 4 cm^{-1} spectral resolution was applied. 100 scans were co-added to every spectrum. To compare the spectra properly the data were normalized using band of CH_2-stretching vibration at 2915 cm^{-1} as a reference (internal thickness band)[28].

Filler flocculation characteristics and vulcanization kinetics of the rubber compounds were studied using a Scarabaeus SIS-V50 rubber process analyzer. A three stage flocculation study was carried out at 120°C and 1.67 Hz. In the first step a high dynamic strain of ~25 % was applied to destroy all the filler agglomerates in the sample. In second stage, a low dynamic shear strain (1.4%) was applied for 2 hours to study the reformation of the filler-filler networks. In the third stage dynamic strain from 0 to 70% was applied to study the Payne effect[29]. The flocculation tendency of silica particles and their strain dependency (Payne effect) were calculated by the following equations,

$$\boldsymbol{Flocculation}\ (\%) = \frac{G'_{120_{min}} - G'_{0_{min}}}{G'_{0_{min}}} \times \mathbf{100} \quad (3)$$

$$\boldsymbol{Amplitude\ of\ payne\ effect} = G'_{0\%} - G'_{70\%} \quad (4)$$

Where, $G'_{120_{min}}$ is the shear modulus at 120 minutes and $G'_{0_{min}}$ is the shear modulus during the beginning of the experiment $G'_{70\%}$ is the modulus at 70% dynamic shear strain and $G'_{0\%}$ is the modulus at ~ 0% dynamic strain. Vulcanization kinetics of the rubber-silica composites were conducted in the same instrument in isothermal time sweep mode at 160°C for 60 minutes.

Measurements of the viscosity of unfilled and filled rubber compounds were carried out in a Mooney viscometer (Montech Rheotechologies, Germany). The conventional large rotor was used and the measurement conditions were ML (1+4) at 100°C. The Mooney viscosity of the rubber compounds were noted at fourth minute of the measurement. The gradient of shear induced viscosity drop (thixotropic behavior) of in-situ silica included rubber compounds were calculated as the difference between the Mooney units at 0 and 4 minutes.

The tensile tests were performed with DIN S2 dumbbell specimens as per the DIN 53504 using Zwick/Roell-Z010 material testing machine with an optical elongation sensor at a cross head speed rate of 200 mm/min at room temperature. The hardness of rubber composites was measured by Bareiss Shore-A hardness tester. The dynamic mechanical analysis of different silica filled composite was performed on a dynamic mechanical thermal spectrometer (Gabo Qualimeter, Ahlden, Germany, model Eplexor-150N) in tension mode. The temperature sweep experiments were performed at a frequency of 10 Hz between -60 ˚C and 80 ˚C with a heating rate of 2 K/min, 0.5% dynamic strain and 1% static strain. The amplitude sweep measurements were performed on Eplexor-2000 N in tension mode at room temperature, at a constant frequency of 10 Hz, 60 % pre-strain and dynamic strain from 0.01-30 %. Hydrodynamic reinforcement values for the samples were calculated using the Guth-Gold model (Eq.5). It is assumed that at high values of dynamic strain there would be no filler-filler interaction and the dynamic modulus of composite will be only influenced by hydrodynamic reinforcement[30]. The experimentally obtained strain sweep values and extrapolated higher strain values are further fitted with Kraus model (Eq. 6) to understand the quantitative information about filler dispersion and filler-filler networks from the strain sweep measurements.

$$\boldsymbol{E_c = E_m(1 + 1.25\varphi + 14.1\varphi^2)} \quad (5)$$

$$\boldsymbol{E'(\gamma_c) = E'_\infty + (E'_i - E'_\infty)/(1 + (\gamma/\gamma_c)^{2m}} \quad (6)$$

E_c and E_c are the low strain dynamic elastic moduli of the composite and pure matrix obtained from dynamic strain sweep measurements, φ is the volume fraction of silica presented in a vulcanizates, $\boldsymbol{\gamma_c}$ is a critical strain amplitude defining the maximum breakdown of filler-filler network (or strain at which the maximum modulus reduction occurs), $\boldsymbol{\gamma}$ is the tensile strain amplitude, $\boldsymbol{E'_i}$ and $\boldsymbol{E'_\infty}$ are the initial and final modulus of rubber composites respectively (here $\boldsymbol{E'_\infty}$ is the modulus extrapolated by Guth-Gold function), m is a strain amplitude (strain sensitivity) constant.

The SEM micrographs were taken using Ultra plus electron microscope from Carl Zeiss NTS GmbH, Oberkochen, Germany, 3 kV, 30 µm aperture size, SE2 detector. The rubber samples were subjected to cyrofracture after exposure in liquid nitrogen. The fractured surface was further sputter coated with 3 nm platinum using BAL-TEC SCD 500 sputter coater and then examined under the SEM at zero tilt angles. The morphology of silica in rubber matrix was investigated by using TEM model JEM 2010 with 120 kV acceleration voltage and bright field illumination. The ultra-thin sections of silica composites were prepared by ultra-microtomy (Leica Ultracut UCT, Leica microsystems GMbH, Wetzlar Germany) at -120 ˚C.

The rebound resilience properties of composites towards free drop pendulum impact force were determined by a resilience tester (Bareiss, Germany) according to DIN 53512, ISO 4662 method at 20°C and 60°C. A circular specimen with 60 mm diameter and 5 mm thickness was utilized for the resilience measurements. The heat build-up experiments were conducted by a dynamic mechanical thermal spectrometer (Eplexor-2000 N, Gabo, Ahlden, Germany). The samples were preconditioned at 50 ˚C for 30 min. The measurement was performed with 1 MPa preload and 4.45 MPa of dynamic compression load for 25 min as per DIN 53533 standards. The solid cylindrical samples of 25 mm height and 17 mm diameter were used for analysis. The heat generated inside the sample was measured by a sharp tip thermocouple and calculated by Eq.7.

$$\textbf{Heat build up}\ (^{\circ}\boldsymbol{C}) = \boldsymbol{T_2 - T_1} \quad (7)$$

Where, $\boldsymbol{T_1}$ and $\boldsymbol{T_2}$ are the core temperatures of the sample before and after the experiment.

The abrasion experiment was performed by DIN rotating drum abrader according to DIN 53516 standard procedure. The disc samples of 16.1 mm diameter and 4.2 mm thickness were used for the abrasion test. The abrasion resistance index (ARI) and relative volume loss ($\Delta \boldsymbol{V_{rel}}$) of SSBR gum and silica filled composites was calculated by Eq.8 and Eq.9.

$$\boldsymbol{ARI} = \frac{\boldsymbol{\Delta m_r \times \rho_t}}{\boldsymbol{\Delta m_t \times \rho_r}} \times \mathbf{100} \quad (8)$$

where, $\boldsymbol{\Delta m_r}$is the mass loss of the standard rubber #1 test piece in mg, $\boldsymbol{\rho_r}$the density of standard rubber #1 in g/cm^3, $\boldsymbol{\Delta m_t}$ the mass loss of the test rubber in mg, and $\boldsymbol{\rho_t}$is the density of the test rubber in g/cm^3.

$$\Delta \boldsymbol{V_{rel}} = \frac{\boldsymbol{\Delta m_t \times \Delta m_{const}}}{\boldsymbol{\rho_t \times \Delta m_r}} \quad (9)$$

$\boldsymbol{\Delta m_{const}}$ is the measured mass loss in standard reference rubber in mg, $\boldsymbol{\Delta m_r}$ is the mass loss of standard rubber test piece in mg, $\boldsymbol{\Delta m_t}$ is the mass loss of test rubber piece in mg, and $\boldsymbol{\rho_t}$ is density of test rubber in mg/cm^3.

The crosslink density of gum and *in-situ* silica filled SSBR composites were investigated by equilibrium swelling method. The volume fraction of rubber (v_r) is determined[31] by Eq.10.

$$\upsilon_r = \frac{\frac{w_d - f_{ins} w_i}{\rho_r}}{\frac{w_d - f_{ins} w_i}{\rho_r} + \frac{w_0}{\rho_s}} \quad (10)$$

Where, w_i, w_s and w_d are the initial weight of samples before swelling, swollen and dried samples after swelling, respectively. w_o is the equilibrium weight of solvent absorbed by the samples. $w_0 = w_s$-w_d, f_{ins} is the weight fraction of the insoluble substances like silica and zinc oxide. The classical Flory-Rehner equation is utilized with regard to the volume fraction to calculate the crosslinking density ($v_{FR} = 1/M_c$). Two types of network models[32] have been proposed to analyze the network structures of cross-linked polymers which are the Affine (Eq.11) and the Phantom network (Eq. 12) model; the equations are as follows.

$$\ln(1-\upsilon_r) + \upsilon_r + \chi \upsilon_r^2 = -\frac{\rho_r}{M_c} V_s \left(\upsilon_r^{1/3} - \frac{2\upsilon_r}{f} \right) \quad (11)$$

$$\ln(1-\upsilon_r) + \upsilon_r + \chi \upsilon_r^2 = -\frac{\rho_r}{M_c} V_s \left(1 - \frac{2}{f} \right) \upsilon_r^{1/3} \quad (12)$$

Hereby, ρ_r is the density of rubber, V_s is the molar volume of toluene, χ is the Flory-Huggins interaction parameter (0.413) for SBR-toluene and f is the crosslink functionality.

Results and discussion

Time dependent silica conversion study

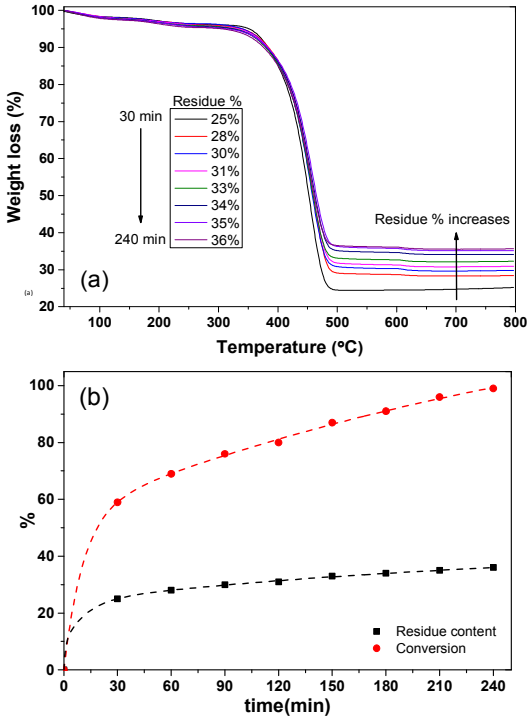

Figure 1. (a) Time dependent silica conversion from TEOS inside the SSBR matrix analyzed by thermogravimetric analysis (b) a percentage of silica conversion and residue with respect to reaction time

The time dependent silica particle growth inside SSBR matrix investigated by thermogravimetric analysis is depicted in Fig. 1a. The final weight obtained above 700 °C is considered as the amount of silica presented in rubber[17]. Fig. 1a shows the increase in amount of residue with time (every 30 min) indicating the conversion of TEOS into silica. Fig. 1b represents the amount of silica in the masterbatch with time calculated as per Eq. 1 and the conversion of silica obtained from Eq. 2. The amount of residue obtained in the first 30 min is ~25 % and the conversion is ~60 %. An overall conversion rate of ~98 % is observed within 240 minutes. For the samples with the highest conversion, almost 2-4 % weight loss is observed between 100 °C and 350 °C and this may be due to the evaporation of

trace catalyst, solvent and TEOS[19]. Fig.2a depicts ATR-FTIR spectra of raw SSBR and TEOS used for the in-situ silica synthesis. For raw SSBR bands are observed at 909 cm^{-1} and 967 cm^{-1}due to wagging vibrations of cis 1,2 and trans 1,4 -CH butadiene groups[33] respectively. In the case of TEOS, a strong band observed at 1070 cm^{-1} represents the stretching vibration of Si-O-C groups. At the same time, multiple bands are observed in the 3000-2800 cm^{-1} region for all pure substances, which pertains to the $-CH_2-$ and $-CH_3$ stretching vibrations[34].

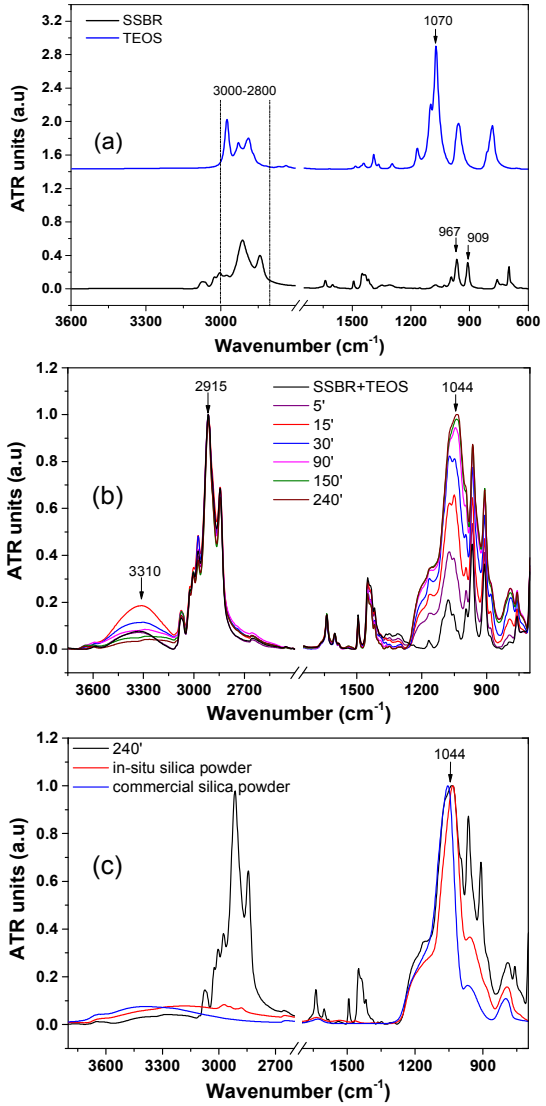

Figure 2. a) ATR-FTIR spectra of pure chemical substances used for in-situ silica synthesis b) Normalized ATR spectra of the solidified reacting mixture as kinetic data of sol-gel reaction c) ATR spectra of pure in-situ silica, commercial silica powder and final reaction mixture at 240 min

The qualitative kinetics of silica particle growth inside the rubber matrix analyzed by ATR-FTIR technique is depicted in Fig.2b. The novel growing band at 1044 cm^{-1} as a function of reaction time can be clearly seen and represents the Si-O-Si stretching vibration of silica oxide that is converted from the TEOS[35]. The silica band at 1044 cm^{-1} is getting more intensive gradually what confirms the silica concentration increase in the SSBR[36]. The second broad band appears in the silica-rubber system around 3310 cm^{-1}, which is not observed for pure TEOS as well as for raw rubber. These broad band corresponds to the stretching vibrations of hydroxyl groups (-OH) from the silica surface or could also be due to the water adsorbed on the surface of the generated silica particles[37]. Fig.2c demonstrates the comparison of ATR spectra of pure in-situ silica powder and final reaction mixture (at 240 min) with ATR-FTIR spectrum of a commercial silica powder. The spectra's coincidence of self-synthesized and commercial silicas (bands appeared around 1044 cm^{-1}) confirms the expected synthesis in rubber system and statement that SSBR rubber is highly filled with silica.

The quantitative determination of *in-situ* silica present in silica-rubber masterbatches estimated by thermogravimetric analysis is presented in Fig. 3. Higher amounts of silica could be produced with the use of higher amount of TEOS and water. In Fig. 3 the amount of residue increases with the increase in amount of TEOS and water. The final weight loss obtained at 800°C is considered as the amount of silica present in the rubber masterbatch. Therefore, from the final weight the amount of in-situ silica present in the system is calculated by Eq. 1 and converted into 'phr'[38]. To cross check the amount of *in-situ* silica in the masterbatches, commercial precipitated silica compounds are prepared with similar volume fraction and subjected to thermal analysis (samples designated as 'x' in fig.3). The experimental result reveals a similar temperature loss profile for both the samples with approximately the same final weight loss. This further confirms the estimated amount of *in-situ* silica in the masterbatches to be around 10-50 phr. Fig.3 demonstrates no weight loss for commercial silica compounds at 100 °C - 350 °C affirming the presence of small amount of catalyst, solvent and TEOS in the *in-situ* silica compounds[19].

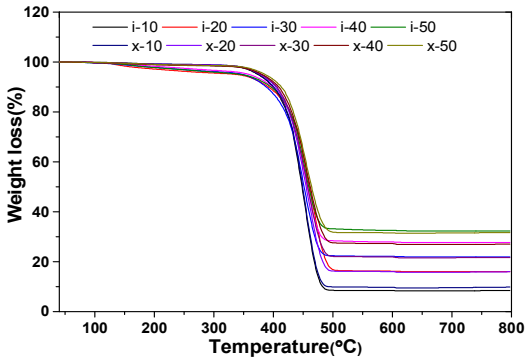

Figure 3. Thermogravimetric analysis of in-situ and commercial silica-rubber masterbatches

Characterization of the rubber compounds

Fig. 4 compares the Mooney viscosities of commercial and *in-situ* silica compounds and extracted data are summarized in Table 1. Gum SSBR shows a lowest value of 59 MU and increases significantly with increase in silica content. *In-situ* silica based SSBR compounds exhibits lower Mooney viscosity compared to commercial silica compounds[39]. A lower Mooney viscosity is always preferred as the compounds display good rheological properties and ease of processing. Mooney viscosity of 50 phr commercial silica (without plasticizers or oil) compound is too high and could not be evaluated as it exceeds the measuring capability of the instrument. The commercial silica particles form a filler-filler network structure resulting in an increase in Mooney viscosity. In contrast, *in-situ* silica particles forms less networks or weak networks and are freely mobile when subjected to shear. Such characteristics could be the reason for the lower viscosity of the *in-situ* compounds. Interestingly, the gradient of viscosity drop under shear stress of *in-situ* and commercial silica compounds are almost similar for the same volume fraction[40]. The filler flocculation and filler-filler networks in silica-rubber masterbatches are investigated to understand the agglomeration and aggregation tendency of the *in-situ* silica particles during processing. It is well known that SSBR and many general purpose rubbers are hydrophobic and silica is hydrophilic in nature. Due to the difference in surface energies between rubber and silica, the silica particles tend to aggregate. Such a tendency of fillers to form aggregates in the rubber is called filler flocculation[29]. This affects the processability and final properties of the compounds to a large extent. Formation of filler networks majorly influence on the elastic modulus of highly filled rubber compounds. To understand such effects, dynamic strain sweep measurements are often conducted. The dynamic filler flocculation and strain dependent filler-filler network characteristics are depicted in Scheme 2.

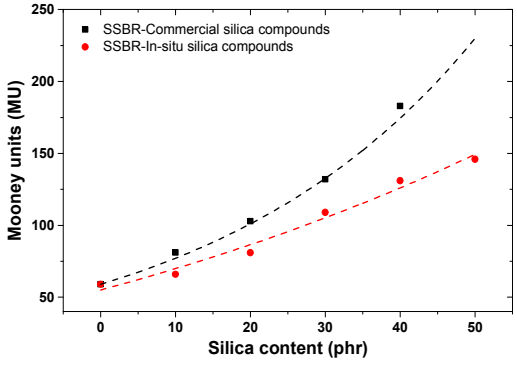

Figure 4. Effect of Mooney viscosity with different silica fraction in SSBR at 100 °C

Fig. 5 shows the three different stages involved in the filler flocculation study. In a first stage, a constant 25 % dynamic strain is applied for 5 min assuming a complete destruction of the filler networks. The dynamic shear modulus is higher for higher volume fractions of silica due to hydrodynamic effect. The experiment is then continued to the second stage with low strain amplitude of 1.4% for 120 min to facilitate filler network reformation. With time, a slow increase in the shear moduli (G') of the filled compounds is evident in Fig. 5. The increase in G' is truly dependent on the volume fraction of the filler and the filler-filler aggregation characteristics. Therefore, high silica content would result in a higher aggregation tendency. Finally in the third stage, the compounds are subjected to strain sweep measurements (Payne effect up to 70% dynamic strain) and the experimental results shows that highly filled silica rubber compounds exhibit faster reduction of the G' values. The rate of flocculation and the amplitude of Payne effect are calculated quantitatively as per Eq.3 and Eq.4 respectively and depicted in Fig.6.

Table 1.Mooney viscosity of varies silica filled SSBR compounds

Samples	Commercial silica			*In-situ* silica		
	MU_0	MU_4	MU_{0-4}	MU_0	MU_4	MU_{0-4}
Gum	80	59	21	80	59	21
10	126	81	45	100	66	34
20	147	103	44	123	82	41
30	177	131	46	156	110	46
40	229	183	46	177	131	46
50	NA	NA	NA	224	147	77

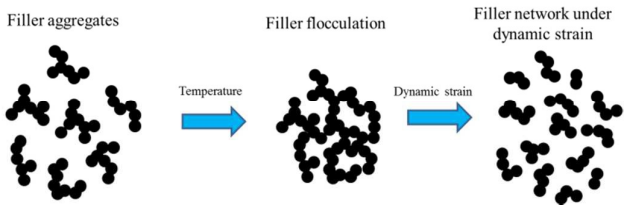

Scheme 2. A schematic representation of filler flocculation and filler-filler network break-down under dynamic strain sweep measurements

Vulcanization characteristics of *in-situ* silica SSBR composites are summarized in Table 2 and their respective cure curves are given in Fig.7. The unfilled SSBR gum compound exhibits higher scorch time (t_2) and optimum cure time (t_{90}), compared to *in-situ* silica filled compounds. Interestingly, the scorch times and optimum cure times of the *in-situ* silica filled composites without silane coupling agent are almost similar for all filler content. The result clearly shows the vulcanization behavior of SSBR not being affected by the increasing amounts of *in-situ* silica. Such results are unique as compared to commercial silica filled compounds which retard the vulcanization reaction at higher filler concentrations leading to higher scorch times and optimum cure times due to its acidic nature[41]. Since *in-situ* silica particles are generated through base catalysis sol-gel reaction, it does not affect the vulcanization kinetics even at

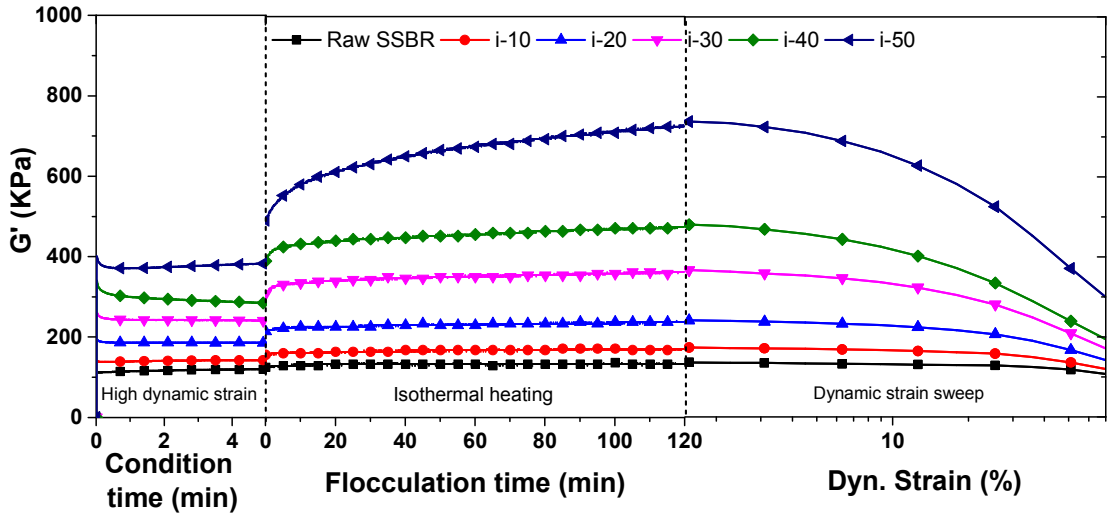

Figure 5. Dynamic filler flocculation and strain sweep measurements

higher concentrations. Meanwhile, in presence of silane coupling agent the scorch times are similar, whereas the composites show higher optimum cure times with increasing silane concentration.

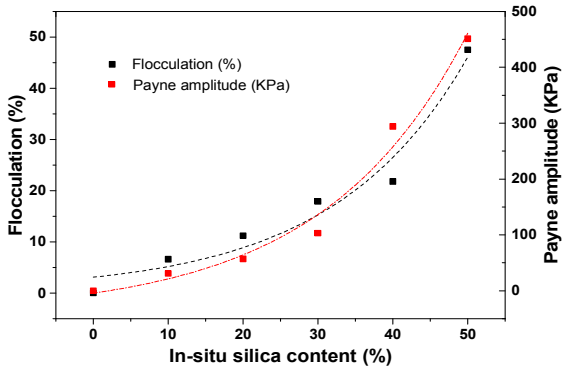

Figure 6. Flocculation and dependent Payne effect of *in-situ* silica-SSBR compounds

The cure rate index (CRI) of the compounds decrease with higher dosage of the silane coupling agent. It is evident that the rate of cure is affected by the incorporation of silane, as higher CRI values are observed in the absence of the silane coupling agent. Therefore, in-situ silica compounds show faster cure characteristics in the absence of silane[8]. The maximum torque (S'max) increases with the amount of in-situ silica in both pristine as well as silane assisted composites. Nevertheless, a higher maximum torque is observed for silane assisted in-situ silica composites. Additionally, pristine in-situ silica compounds exhibit reversion signifying a higher proportion of polysulfidic crosslink bridges.

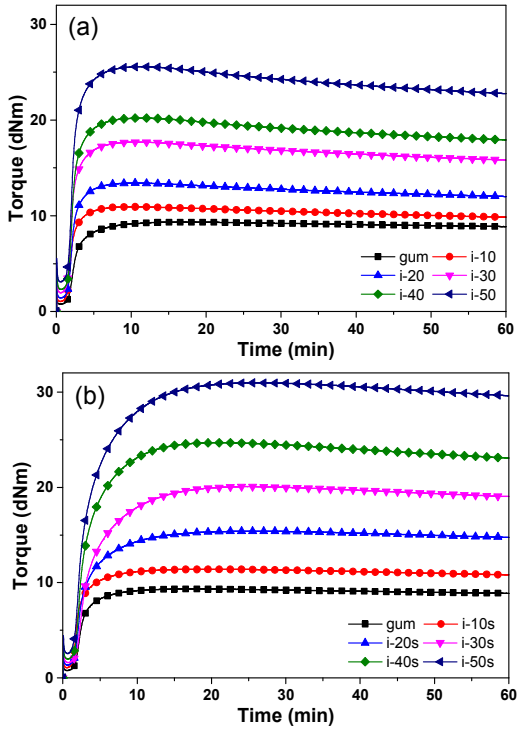

Figure 7.Vulcanization curves of SSBR/*in-situ* silica composites (a) absence and (b) presence of silane coupling agent

Mechanical and dynamic mechanical properties

The stress-strain characteristics of *in-situ* silica in presence and absence of silane coupling agent are analyzed by tensile measurements are tabulated in table 3 and depicted in Fig.8. The tensile strength and modulus of SSBR composites are improved significantly by the *in-situ* silica. The stress-strain

behavior of the filled composites in absence of silane coupling agent show gradual increase in moduli and tensile strength compared to the unfilled vulcanizate. However, the stress-strain plots do not follow any pattern at higher silica loadings indicating higher anisotropy in the composites. Nevertheless, the composites with silane coupling agent offer better filler-polymer interactions, exhibiting huge improvements in moduli and tensile strength. Unfortunately, as a consequence of better filler-polymer interaction by silane, the stiffness of matrix increases compromising the elongation at break. Moreover, the stress-strain plots of *in-situ* silica composites with silane display higher modulus in the low strain region also behaving like Hookean materials. To quantify the amount of reinforcement enhanced by the silica particles, the reinforcing efficiency(RE)[14] is estimated by

$$RE = \frac{M_{100\%\,filled} - M_{100\%\,gum}}{wt\%\ of\ silica}.$$

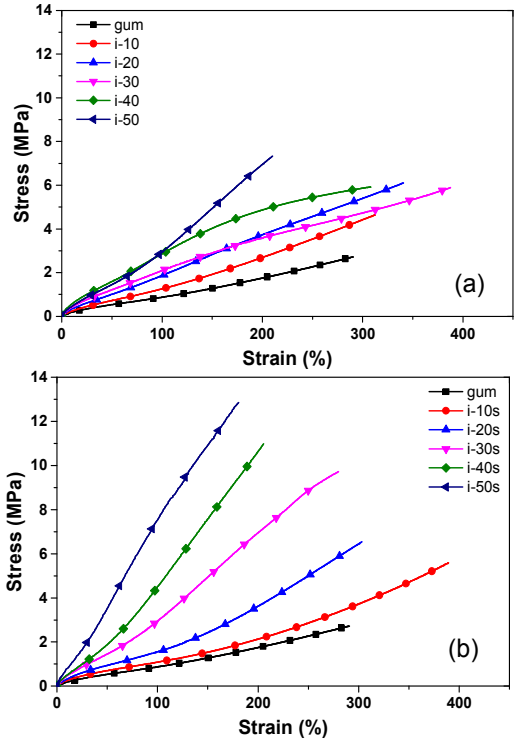

Figure 8. Tensile properties of SSBR/*in-situ* silica composites in (a) absence and (b) presence of silane coupling agent

The dynamic mechanical properties of unfilled SSBR and its *in-situ* silica composites studied over a temperature range of -60 °C to 80 °C are depicted in Fig. 9 and various important parameters are summarized in Table 4. Fig. 9(a, c) illustrates the gradually increasing storage moduli of the *in-situ* silica composites according to the silica fraction. From Table 4, improvements in the dynamic mechanical properties of *in-situ* silica composites due to enhanced filler-polymer interaction by the silane coupling agent could be visualized. Fig. 9b and Fig. 9d shows the tan δ plot for the *in-situ* silica SSBR composites. It is well known that addition of silica in rubber reduces tan δ_{max} values and further reduction would be observed upon incorporation of silanes[42]. In Fig. 9b the glass transition temperature (T_g) is slightly shifted to higher temperatures for all the composites. But in Fig. 9d, i.e. with the of presence of silane coupling agents, the T_g shifts are significant[14]. This result confirms that silica-rubber interface is substantially improved by effective silanization as well as by formation of strong nano layer of immobilized rubber chains around the silica surface[29]. Thus restricted mobility of rubber chains by silane modified silica surface causes the shift in T_g[43]. From the temperature sweep studies, *in-situ* silica reinforces the SSBR matrix very well and dynamic behavior of the composites are further improved with the presence of coupling agents[18].

Table 2. Vulcanization characteristics of SSBR/*in-situ* silica composites

Samples	t_2 (min)	t_{90} (min)	S' min (dNm)	S' max (dNm)	CRI (min^{-1})
Gum	2.35	5.56	0.78	9.34	31.15
i-10	2.05	4.11	1.06	10.95	48.54
i-20	2.11	4.00	1,42	13.43	52.91
i-30	1.59	4.19	1,96	17.7	38.46
i-40	2.05	4.11	2,31	20.21	48.54
i-50	1.59	4.10	3,11	25.58	39.84
i-10s	1.56	5.33	0,99	11.6	26.52
i-20s	2.23	9.23	1,32	15.38	14.28
i-30s	2.01	11.12	1,58	20.03	10.76
i-40s	2.17	12.10	2,01	24.69	10.07
i-50s	1.59	13.45	2,89	30.98	8.43

Table 3. Stress-strain properties of SSBR/*in-situ* silica composites

Samples	M100% (MPa)	M200% (MPa)	M300% (MPa)	TS (MPa)	RE (%)	EB (%)	HRD (shore A)
Gum	0.87	1.76	-	2.72	-	290	42
i-10	1.27	2.69	4.42	4.65	4.59	310	48
i-20	1.87	3.73	5.40	6.10	6.25	340	53
i-30	2.10	3.59	4.73	5.88	5.53	390	56
i-40	2.87	4.87	5.87	5.92	7.24	308	60
i-50	2.93	6.98	-	7.53	6.38	449	63
i-10s	1.08	2.13	3.72	5.58	2.43	390	48
i-20s	1.56	3.62	6.45	6.53	4.38	305	54
i-30s	2.95	6.95	-	9.72	9.57	280	59
i-40s	4.25	-	-	10.98	12.58	205	61
i-50s	7.53	-	-	12.5	21.31	180	68

*M-Modulus at, TS-Tensile strength, RE-Reinforcing efficiency, EB-Elongation at break, HRD-Hardness

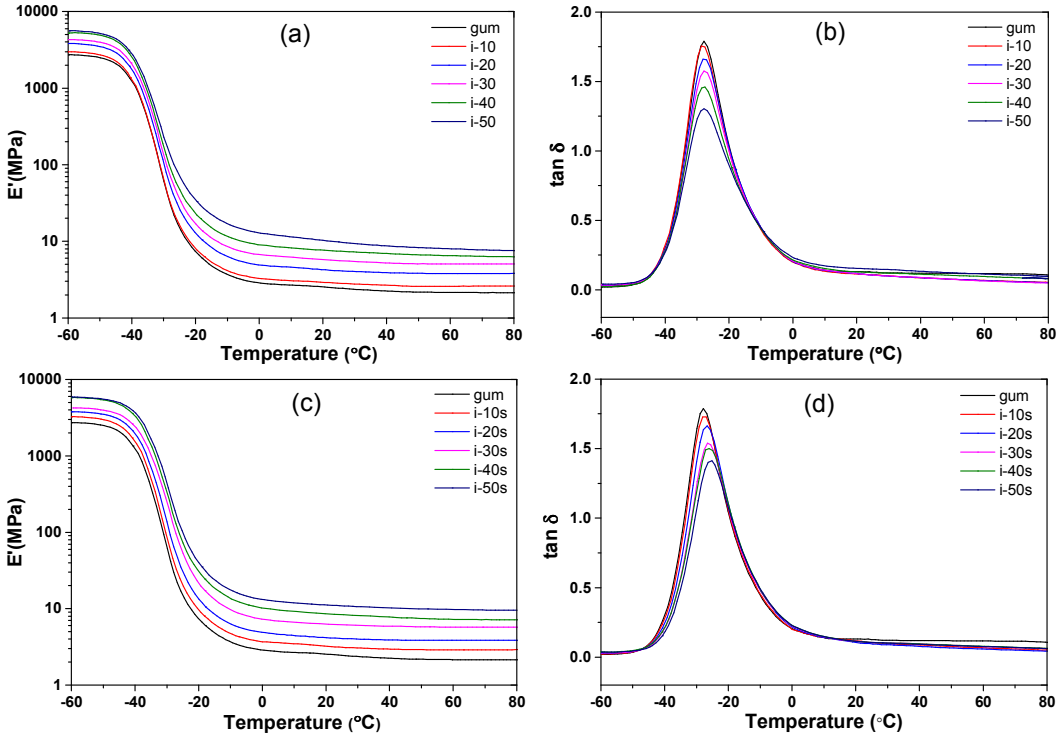

Figure 9. Dynamic mechanical temperature sweep analysis of *in-situ* silica-SSBR nanocomposites. (a) & (c) storage modulus and (b) & (d) tan δ graph for SSBR/*in-situ* silica composites in absence and presence of coupling agent

Table 4. Dynamic mechanical properties of SSBR/*in-situ* silica composites

Samples	E' @ 0°C (MPa)	E' @ 25°C (MPa)	E' @ 60°C (MPa)	tan δ_{max}	T_g (°C)
Gum	2.85	2.44	2.14	1.78	-27.8
i-10	3.29	2.90	2.59	1.74	-27.5
i-20	4.88	4.13	3.79	1.65	-27.0
i-30	6.58	5.58	5.05	1.56	-26.7
i-40	9.05	7.41	6.48	1.51	-27.1
i-50	12.78	9.81	7.97	1.49	-27.5
i-10s	3.68	3.12	2.89	1.72	-27.0
i-20s	6.06	5.33	5.06	1.61	-26.8
i-30s	7.20	6.12	5.74	1.53	-26.5
i-40s	10.2	8.32	7.26	1.51	-26.0
i-50s	13.2	10.85	9.75	1.41	-25.2

Table 5. Calculated strain dependent dynamic properties of composites by Kraus function

Samples	$E_i' - E_\infty'$ (MPa)		Critical strain (γ_c) %		Amplitude constant (m)	
	In-situ w/o silane	*In-situ* with silane	*In-situ* w/o silane	*In-situ* with silane	*In-situ* w/o silane	*In-situ* with silane
Gum	0.22	-	-	-	-	-
10	0.42	1.04	55.06	53.53	0.54	0.53
20	1.70	2.12	53.24	53.38	0.50	0.48
30	3.30	4.60	42.97	41.93	0.48	0.46
40	4.98	5.99	39.48	40.85	0.49	0.45
50	7.23	8.34	30.59	35.92	0.47	0.43

*w/o defines without

The dynamic mechanical strain sweep measurements also known as 'Payne effect' are performed to understand the filler-filler interaction and strain induced softening of the composites. The obtained experimental results are fitted with Kraus equation (Eq. 6) by extrapolating to 1000 % strain; where only hydrodynamic reinforcement exists (see Eq. 5). The results are plotted in Fig. 10 and the quantitative information about the Payne effect is tabulated in Table 5.

In Fig. 10, the solid lines represent samples without silane and dotted lines represent the presence of silane coupling agents in the Kraus fitting function[44]. As the volume fraction of silica is increased in the rubber matrix, a well percolated filler-filler networks are formed. With the incorporation of silane coupling agent, the *in-situ* silica rubber compounds display an increase in the dynamic storage modulus. This effect is contrary to commercial precipitated silica filled composites; as silane incorporation reduces the storage modulus[18]. Similar

effects (increase in dynamic modulus) are usually observed for carbon nanotubes filled system[45, 46]. However, Payne effect is observed for the *in-situ* silica compounds both in the presence and absence of silane coupling agent. At the same time, the critical strain value (γ_c) of the composites reduces with increase in silica fraction. Such behavior indicates a higher dependency of the filler networks towards dynamic strain as the filler fraction increases. The silane incorporated composites show less strain dependency by displaying higher critical strain values, meaning the filler networks are less susceptible to the dynamic strain. Accordingly, silane incorporation significantly improves the dynamic performance of the composites by improving the filler-polymer interaction. The amplitude constant (*m*) constantly decreases with increase in filler content and lies in-between 0.43 to 0.54[44].

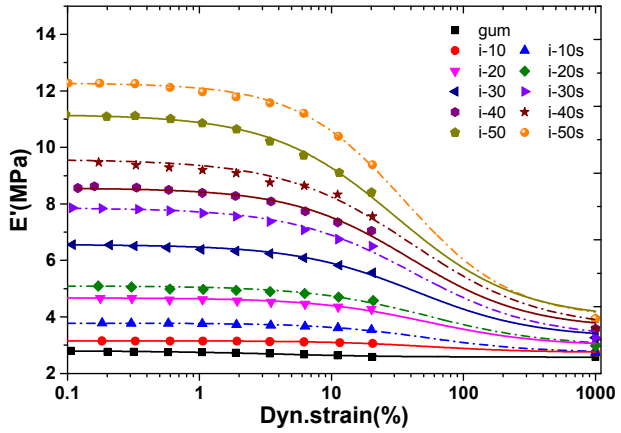

Figure 10. Strain dependency of dynamic elastic modulus for the SSBR/*in-situ* silica composites (symbols represent experimental data and lines represent the fitted Kraus equation)

Rubber performance

Some important rubber performance parameters like rebound resilience, heat buildup, abrasion, swelling in solvent is also evaluated and obtained results are depicted in Fig. 11 and Fig. 12. At room temperature, the resilience values are found to be reducing with increase in the amount of fillers (Fig. 11a). At the same time, resilience properties are greatly improved with the addition of silane in the *in-situ* silica composites[19]; even the high temperature (60˚C) resilience properties are improved.

The heat build-up properties of *in-situ* silica filled SSBR composites in presence and absence of silane coupling agent are investigated as per Eq. 7 and plotted in Fig. 11b. The unfilled gum vulcanizate shows the least heat build-up inside the core of the sample. At the same time, as the amount of silica fraction increases in the SSBR, the degree of heat generation and build-up inside the composites is increases significantly. Inclusion of rigid particles in a viscoelastic material would exhibit excessive heat generation by increasing the internal friction due to poor filler polymer interaction and a lower heat loss[47]. Eventually, incorporation of silane coupling agent in the silica filled system reduces heat generation and increases the heat loss of the material by improving the filler-polymer interaction due to silanization[14].

The abrasion properties of *in-situ* silica filled SSBR compounds are plotted in Fig. 11c and Fig. 11d. The abrasion resistance index (calculated by Eq. 8) clearly depicts the improved resistance of the composites towards friction with the addition of *in-situ* silica. At the same time, addition of silane coupling agent results in better resistance towards abrasion. The silane improves the abrasion characteristics through better filler-polymer interaction. The relative volume loss (calculated by Eq. 9) is also significantly reduced by increasing the silica fraction and silane coupling agent.

The crosslink densities of gum and *in-situ* silica filled SSBR composites are calculated by equilibrium swelling based Flory-Rehner equations Eq. 11 and Eq. 12. The estimated crosslink densities based on affine and phantom network model are depicted in Fig. 12a. The crosslink density of SSBR gradually increases with the volume fraction of silica. Also, the silane coupled *in-situ* silica composites exhibit higher crosslink densities, compared to the unsilanized composites[14]. The enhanced crosslink density of silane incorporated SSBR composites is due to the adsorbed silane coupling agent on the surface of the filler and improved filler-rubber interaction. This improves the filler-polymer interaction through covalent bonding between the rubber and silica surface[48]. The crosslink densities predicted by the Affine network model is lower than by the Phantom network model in both silane and silane free systems. Fig.12b shows the plot of crosslink density obtained from phantom network model against the glass transition temperature (T_g) measured by the dynamic mechanical analyzer (DMA). Linearity is observed between crosslink density and T_g with increasing volume fraction of filler. In the absence of silane the obtained slope is 2.0, however with the incorporation of silane a higher slope of 3.5 is observed. This confirms that crosslink density and T_g of composites are majorly dependent on the silanization reaction as well as filler volume fraction. This correlation further evidences the enhanced silica-rubber interaction by the silane.

Morphology

To understand the in-situ silica-rubber interaction and interfacial adhesion in presence and absence of silane coupling agent, fracture surface of the composites are analyzed by SEM. In Fig. 13a, the 30 phr in-situ silica composite without silane shows aggregated particles with average particle size of around 200-300 nm. The fracture surface shows some kind of holes, which represent the poorly adhered particles being pulled out from the matrix during cryo-fracture. In Fig.13b, by presence of coupling agent, the in-situ silica the particles are fully covered by rubber layers. The micrograph signifies the superior adhesion of the in-situ silica fillers with the rubber matrix as a benefit of the silane coupling agent. The particle size and dispersion of silica nanoparticles in rubber matrix is one of the most critical parameters, which determine the overall performance of the nanocomposite.

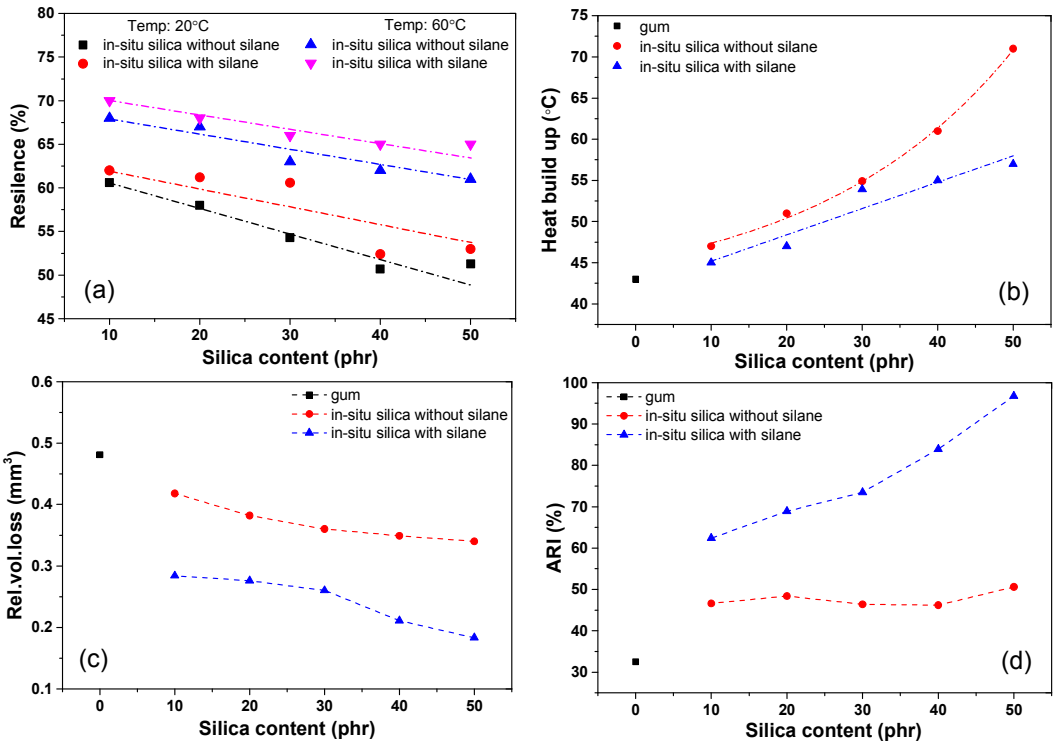

Figure 11. a) Rebound resilience characteristics, b) Heat build-up properties, c) Relative volume loss, and d) Abrasion resistance index (ARI) % of *in-situ* silica filled SSBR composites

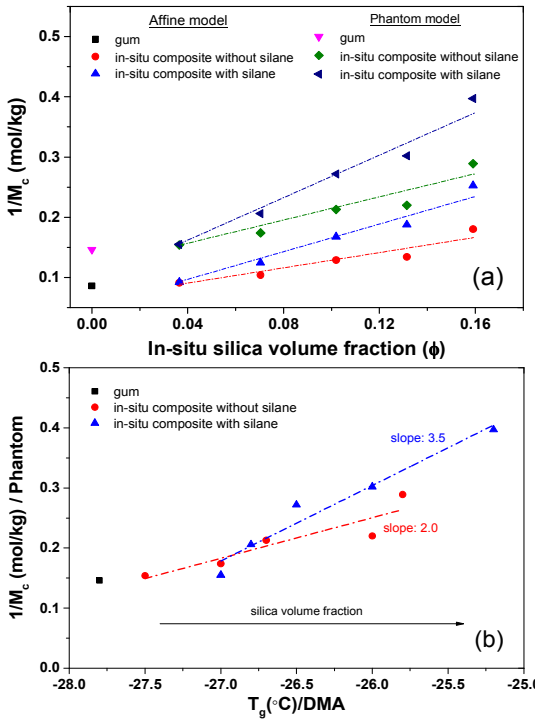

Figure 12. a) Effect on crosslink density of SSBR with respect to silica fraction and silane b) the correlation between T_g and crosslink density

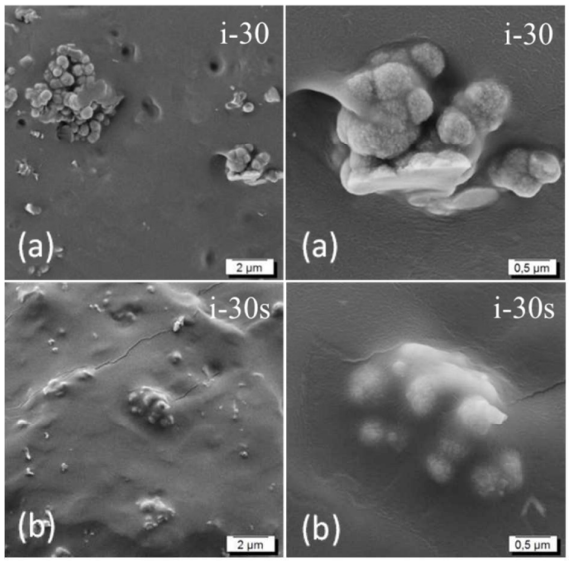

Figure 13. SEM micrographs of cryo-fracture failure surface investigation of *in-situ* silica composites (a) absence and (b) presence of TESPT silane coupling agent at low and high magnifications

Aggregates and agglomerates of filler particles in a rubber matrix act as stress concentration points resulting in early failure. Fig.14 displays the TEM images of silane coupled SSBR/*in-situ* silica composites. The silica particles are moreover

individual and bigger in size with average particle size of around 200 to 300nm. Silane coupling agents improve the dispersion of silica particles and some particles that exist interconnected during synthesis.

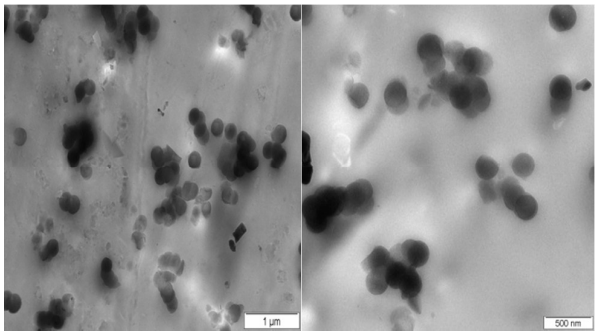

Figure 14. TEM images of silane modified SSBR/*in-situ* silica composites

Conclusions

In-situ synthesis of silica nanoparticles in SSBR matrix was done successfully by sol-gel method. In-situ silica composites offered improved dynamic mechanical properties, lower heat buildup, higher rebound resilience, better processability and abrasion characteristics in the presence of silane coupling agent. In comparison to existing literature, current approach promises (a) an improved state of silica dispersion (b) higher amounts of silica loading into the rubber without sacrificing the processability (c) better way to control and customize the particle size and distribution (d) industrial feasibility (e) possible way to save mixing energy due to easy incorporation. Currently, the focus is being laid to understand the reinforcement mechanism of in-situ silica in the rubber on the basis of (i) surface activity[24], (ii) particle distribution, (iii) trapped rubber chains inside the silica particles[12] and (iv) the physical and chemical interactions. Detailed study of the results will be communicated in the forthcoming publications.

Acknowledgements

The authors are thankful to Dr. K. J. Eichhorn for FTIR discussion and Mrs. S. Krause for TGA analysis.

Notes and references

1. E. M. Dannenberg, *Rubber Chemistry and Technology*, 1975, **48**, 410-444.
2. J.-B. Donnet and A. Voet, *Carbon black: physics, chemistry, and elastomer reinforcement*, M. Dekker, 1976.
3. G. Kraus, *Rubber Chemistry and Technology*, 1978, **51**, 297-321.
4. M. Klüppel and G. Heinrich, *Rubber Chemistry and Technology*, 1995, **68**, 623-651.
5. S. Rooj, A. Das, K. W. Stöckelhuber, D.-Y. Wang, V. Galiatsatos and G. Heinrich, *Soft Matter*, 2013, **9**, 3798.
6. A. Das, R. Jurk, K. W. Stöckelhuber and G. Heinrich, *Macromolecular Materials and Engineering*, 2008, **293**, 479-490.
7. S. B. Eshwaran, D. Basu, S. R. Vaikuntam, B. Kutlu, S. Wiessner, A. Das, K. Naskar and G. Heinrich, *Journal of Applied Polymer Science*, 2015, **132**.
8. V. Raman, S. Rooj, A. Das, K. Stöckelhuber, F. Simon, G. Nando and G. Heinrich, *Journal of Macromolecular Science, Part A*, 2013, **50**, 1091-1106.
9. U. Goerl, A. Hunsche, A. Mueller and H. Koban, *Rubber chemistry and technology*, 1997, **70**, 608-623.
10. S. Wolff, *Rubber Chemistry and Technology*, 1996, **69**, 325-346.
11. N. Vleugels, W. Pille-Wolf, W. K. Dierkes and J. W. M. Noordermeer, *Rubber Chemistry and Technology*, 2015, **88**, 65-79.
12. E. Miloskovska, C. Friedrichs, D. Hristova-Bogaerds, O. Persenair, M. van Duin, M. R. Hansen and G. de With, *Macromolecules*, 2015, **48**, 1093-1103.
13. F. Bohin, I. Manas-Zloczower and D. Feke, *Rubber chemistry and technology*, 1994, **67**, 602-609.
14. A. Hashim, B. Azahari, Y. Ikeda and S. Kohjiya, *Rubber chemistry and technology*, 1998, **71**, 289-299.
15. P. Cassagnau, *Polymer*, 2003, **44**, 2455-2462.
16. J. Ramier, C. Gauthier, L. Chazeau, L. Stelandre and L. Guy, *Journal of Polymer Science Part B: Polymer Physics*, 2007, **45**, 286-298.
17. S. Kohjiya and Y. Ikeda, *Rubber chemistry and technology*, 2000, **73**, 534-550.
18. A. Das, R. Jurk, K. Werner Stöckelhuber and G. Heinrich, *Journal of Macromolecular Science, Part A: Pure and Applied Chemistry*, 2007, **45**, 101-106.
19. S. Kohjiya, K. Murakami, S. Iio, T. Tanahashi and Y. Ikeda, *Rubber chemistry and technology*, 2001, **74**, 16-27.
20. S. Prasertsri and N. Rattanasom, *Polymer Testing*, 2011, **30**, 515-526.
21. B. Chaichua, P. Prasassarakich and S. Poompradub, *Journal of Sol-Gel Science and Technology*, 2009, **52**, 219-227.
22. Y. Ikeda and S. Kohjiya, *Polymer*, 1997, **38**, 4417-4423.
23. E. Miloskovska, E. Nies, D. Hristova-Bogaerds, M. van Duin and G. de With, *Journal of Polymer Science Part B: Polymer Physics*, 2014, **52**, 967-978.
24. E. Miloskovska, M. R. Hansen, C. Friedrich, D. Hristova-Bogaerds, M. van Duin and G. de With, *Macromolecules*, 2014, **47**, 5174-5185.
25. L. Bokobza and J.-P. Chauvin, *Polymer*, 2005, **46**, 4144-4151.
26. Y. Ikeda, S. Poompradub, Y. Morita and S. Kohjiya, *Journal of Sol-Gel Science and Technology*, 2008, **45**, 299-306.
27. Y. Ikeda, A. Tanaka and S. Kohjiya, *Journal of Materials Chemistry*, 1997, **7**, 1497-1503.
28. J. L. Koenig, *Spectroscopy of polymers*, Elsevier, 1999.
29. K. W. Stöckelhuber, A. S. Svistkov, A. G. Pelevin and G. Heinrich, *Macromolecules*, 2011, **44**, 4366-4381.
30. G. Heinrich, M. Klüppel and T. A. Vilgis, *Current opinion in solid state and materials science*, 2002, **6**, 195-203.
31. J. L. Valentín, I. Mora-Barrantes, J. Carretero-González, M. A. López-Manchado, P. Sotta, D. R. Long and K. Saalwächter, *Macromolecules*, 2010, **43**, 334-346.
32. A. Vieyres, R. Pérez-Aparicio, P.-A. Albouy, O. Sanseau, K. Saalwächter, D. R. Long and P. Sotta, *Macromolecules*, 2013, **46**, 889-899.
33. V. M. Litvinov and P. P. De, *Spectroscopy of rubbers and rubbery materials*, iSmithers Rapra Publishing, 2002.
34. G. Socrates, *Journal of the American Chemical Society*, 1995, **117**, 1671-1671.
35. J. Martinez, F. Ruiz, Y. V. Vorobiev, F. Pérez-Robles and J. González-Hernández, *Journal of Chemical Physics*, 1998, **109**, 7511-7514.
36. M. L. Kralevich and J. L. Koenig, *Rubber Chemistry and Technology*, 1998, **71**, 300-309.
37. A. Beganskienė, V. Sirutkaitis, M. Kurtinaitienė, R. Juškėnas and A. Kareiva, *Mater Sci (Medžiagotyra)*, 2004, **10**, 287-290.
38. Y. Ikeda and Y. Kameda, *Journal of sol-gel science and technology*, 2004, **31**, 137-142.
39. S. Mihara, R. Datta and J. Noordermeer, *Rubber Chemistry and Technology*, 2009, **82**, 524-540.
40. N. K. Dutta and D. Tripathy, *Journal of applied polymer science*, 1992, **44**, 1635-1648.
41. P. Pal and S. De, *Rubber Chemistry and Technology*, 1982, **55**, 1370-1388.
42. Y. Ikeda, A. Tanaka and S. Kohjiya, *J. Mater. Chem.*, 1997, **7**, 455-458.
43. G. Tsagaropoulos and A. Eisenberg, *Macromolecules*, 1995, **28**, 6067-6077.
44. G. Heinrich and M. Klüppel, in *Filled Elastomers Drug Delivery Systems*, Springer, 2002, pp. 1-44.
45. A. Das, K. Stöckelhuber, R. Jurk, M. Saphiannikova, J. Fritzsche, H. Lorenz, M. Klüppel and G. Heinrich, *Polymer*, 2008, **49**, 5276-5283.
46. K. Subramaniam, A. Das and G. Heinrich, *Composites Science and Technology*, 2011, **71**, 1441-1449.
47. M. P. Wagner, *Rubber Chemistry and Technology*, 1976, **49**, 703-774.
48. S.-J. Park and K.-S. Cho, *Journal of colloid and interface science*, 2003, **267**, 86-91.